Lab on a Chip

PAPER

View Article Online
View Journal | View Issue

Cite this: *Lab Chip*, 2024, **24**, 3528

A high-sensitivity lab-on-a-chip analyzer for online monitoring of nitrite and nitrate in seawater based on liquid waveguide capillary cells†

Zeming Yang,[ab] Junxiao Zhang,[bc] Jincheng Zhao,[ad] Wen Zhou,[a] Yuanyue Cheng,[a] Zhantang Xu,[a] Panpan Wei,[ad] Zihui Wang,[ad] Haorui Liang[c] and Cai Li *[a]

Optical detection is an indispensable part of microfluidic systems for nutrient determination in seawater. Coupling total internal reflection capillaries with microfluidic chips is a practical alternative to increase the optical path length for high-sensitivity and a low detection limit in colorimetric assays, which has not been applied in microfluidic devices for seawater nutrients. Here, we present an online microfluidic system which integrated a total internal reflection capillary made of Teflon AF 2400 for the high-sensitivity detection of nitrite and nitrate in seawater. The off-chip capillary lengthens the optical path without changing the internal flow path of the microfluidic chip, enhancing the sensitivity, reducing the detection limit and widening the dynamic range of the system, which significantly improves the performance of the microfluidic system based on wet-chemistry. The detection limit for nitrite is 0.0150 μM using an external 20 cm capillary and 0.0936 μM using an internal 5 cm absorption cell, providing an over 6-fold improvement. Laboratory analysis of surface seawater samples collected from the South China Sea with this system and a one-month online deployment of an autonomous analyzer developed based on this system at a station revealed correlations between the nitrite and nitrate with tide, salinity and chlorophyll over slight variations and narrow ranges, demonstrating the high-sensitivity of this method.

Received 20th March 2024,
Accepted 16th June 2024

DOI: 10.1039/d4lc00248b

rsc.li/loc

1 Introduction

Lab-on-a-chip (LoC or microfluidics) technology possesses the potential to shrink the entire laboratory system to a chip scale,[1] facilitating the automation of sophisticated chemical manipulation and liquid handling, enabling volume and weight reduction of the physical dimensions of devices,[2,3] is a powerful alternative to conventional analytical techniques and an indispensable tool to the on-going trends toward the miniaturization of analyzers.[2,4] LoC has been used for water analysis since the late 1990s[5–8] and was developed rapidly for environmental water monitoring thereafter.[4,9,10] In recent years, LoC has been applied for seawater measurements and ocean observation to elucidate the marine biogeochemical properties.[2,11,12] Miniaturization and high-integration were realized in marine chemical sensors and analyzers by LoC to make them portable and deployable to achieve *in situ*[3,13–18] and laboratory[19] determination of seawater nutrients for profile detection and long-term monitoring, which promotes spatiotemporal resolution compared to conventional analytical techniques.

Optical detection is one of the integral parts in the colorimetric systems of LoC-based nutrient devices. Applying planar waveguides based on total internal reflection (TIR) and embedding waveguide optics into the microchannel to increase the optical path length of the absorption cell[20,21] have been used in LoC systems to achieve high-sensitivity and a low limit of detection (LOD). By virtue of the characteristic of sharing the same physical volume with the fluidic channel, the liquid-core waveguide (LCW) reduces the complexity of the microchip design and fabrication and the optical loss during transmission,[22] which are convenient and low cost for the implementation of TIR-based waveguides in LoC systems.

The refractive index of Teflon AF (amorphous fluoropolymers) is 1.29–1.31, which is lower than that of

[a] *State Key Laboratory of Tropical Oceanography, South China Sea Institute of Oceanology, Chinese Academy of Sciences, Guangzhou, 511458, P.R. China. E-mail: liclaire@scsio.ac.cn*
[b] *Key Laboratory of Marine Environmental Survey Technology and Application, Ministry of Natural Resources, Guangzhou, 510310, P.R. China*
[c] *South China Sea Marine Survey Center, Ministry of Natural Resources, Guangzhou, 510310, P.R. China*
[d] *University of Chinese Academy of Sciences, Beijing, 100049, P.R. China*
† Electronic supplementary information (ESI) available. See DOI: https://doi.org/10.1039/d4lc00248b

water (1.33),[23] making it a suitable material for LCWs and it is widely adopted in spectroscopic detection for environmental applications,[24,25] including nutrients analysis in natural waters for *in situ* and online detection.[26–28] Wide application of Teflon AF at the chip scale was commenced in the early twenty-first century and can be broadly classified into two categories according to the application method: coating Teflon AF on a substrate as a cladding layer and connecting commercially available Teflon AF capillaries as liquid waveguide capillary cells (LWCCs). Teflon AF has been coated on PDMS (polydimethylsiloxane),[29,30] silicon[31,32] and glass[33] chips for various purposes, and this requires complicated fabrication procedures and most of the applications occur in digital microfluidics for rendering the hydrophobic layer.[34] Connecting Teflon AF capillaries to microchips, by contrast, requires fewer procedures and is suitable in optical detection LoC systems for improving sensitivities, as well as eliminating the interference from stray light without specific surface treatment on the chip. Capillaries made of Teflon AF 1600 and AF 2400 have been connected with glass chips *via* bonds, adhesive tapes or epoxies[35–40] as the detection cell.

As a practical alternative to increase the optical path length for high-sensitivity and low LOD in colorimetric assay microfluidic systems, connecting Teflon AF capillaries has not hitherto been applied in LoC devices for nutrients determination in seawater. In this work, an online LoC analyzer integrating an LWCC made of Teflon AF 2400 for the high-sensitivity detection of nitrite and nitrate (NO_x^-) in seawater was presented. The micromixer of the chip consists of two serpentine channels to conduct the sequential injection analysis (SIA) for fast measurements. The connection between the LWCC and the chip was realized by a screw joint, which is more convenient to assemble with zero dead volume compared with connections by bonds or epoxies. In addition, the replacement or maintenance of a new, shorter or longer LWCC is more simple and lower-cost based on this coupling approach. By this means the optical path length was greatly elevated and hence the LOD and sensitivity of the LoC system in this work were significantly improved. The LOD using a 20 cm LWCC is 0.0150 μM for nitrite, more than six times lower than that of 0.0936 μM of the internal 5 cm absorption cell. Measurements of the surface seawater samples collected from a scientific cruise with the NO_x^- detection system show a covariation of NO_x^- with chlorophyll. The high-sensitivity capability of the system for minute ranges of variation in biochemical parameters is further demonstrated by a subsequent one-month continuous deployment of an autonomous analyzer at a coastal station and corresponding correlation analysis.

2 Experimental section

2.1 System description

An 8 mm-thick and a 6 mm-thick PMMA (polymethyl methacrylate) plate were machined by micromilling and then bonded to form the microchip (Keyto Fluid Control Co., Ltd., China). The fluidic pathway and control diagram of the system and 3D model of the chip are shown in Fig. 1. The chip photo is given in Fig. S1 of the ESI.†

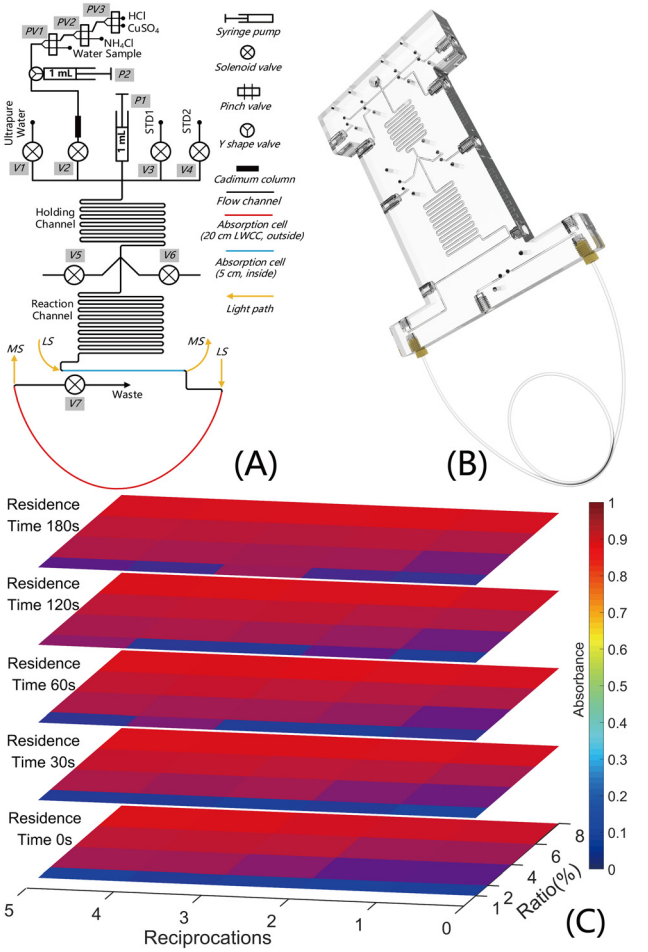

Fig. 1 (A) Fluidic pathway and control diagram of the NO_x^- system. (B) 3D model of the microfluidic chip (with an external LWCC). (C) Orthogonal experiment results with the internal 5 cm absorption cell for the NO_2^- system.

Seven 2-way solenoid valves (1013-22-ELB-5N, Keyto Fluid Control Co., Ltd., China) mounted onto the chip, three 2-way pinch valves (P20T24-01#, Beion Fluid Systems (Shanghai) Co., Ltd., China) and two high-precision 1 mL syringe pumps (S60H1000-24, Beion Fluid Systems (Shanghai) Co., Ltd., China) were integrated to achieve fluidic control.

The microfluidic platform incorporates one internal 5 cm absorption cell and one external LWCC. The LWCC is connected to the internal channel of the chip by the same approach as the commonly used fluid connections, *via* a 1/4-28 threaded fitting, an inverted cone pressure ring made of PFA (polyfluoroalkoxy) and a Teflon gasket. In this case, the LWCC (Biogeneral Inc., USA) made of AF 2400 used was 20 cm in length with an internal diameter (I.D.) of 1 mm, and to retain an equivalent Reynolds number (Re) and a consistent *laminar* flow at the interface between the channel and LWCC, all channels patterned in the chip are circular with an I.D. of 1 mm. All fluid ingresses and egresses on the chip are 1/4-28

threaded holes, which are the same as the LWCC connection, to make it convenient for assembling, replacement and maintenance. The spectrophotometric detection system for each absorption cell comprises a light source (LS-1, Wyoptics, China), two optical fibers (Sun Telecom, China), a customized narrow-band optical filter (GNPF545, Phtode, China) with a peak at 545 nm and a bandwidth of 10 nm and a microspectrometer (ATP1010, Optosky Photonics Inc., China).

2.2 Methods and reagents

The Griess assay is the mainstay and gold-standard for colorimetric nitrite analysis[41–43] and this was adopted in this work. In this assay, nitrite is reacted with an aromatic amine (sulfanilamide) to form a diazonium compound, which is then coupled with a second aromatic amine (*N*-ethylenediamine dihydrochloride, abbreviated to N.E.D.) to produce an azo dye. The product is quantified by spectrophotometry at a wavelength of 543 nm and the absorbance is calculated based on the Beer–Lambert law:

$$A_t = \lg\left(\frac{I_0}{I_t}\right) \quad (1)$$

where A_t is the absorbance with time, and I_0 and I_t are defined in steps 3 and 7 in Table S1 (Section S4, ESI†). Reagents preparation was described previously[44] and is also listed in Section S2 of the ESI.† The nitrate analysis in this system adopted the most well-established and widely used method, the copperized cadmium reduction method.[18,41,45]

2.3 Analytical procedures for fast mixing

The micromixer in this study consists of two serpentine channels for reagents holding and reaction (Fig. 1A). The SIA regime was applied for fast mixing in the micromixer. The control protocol for the pumps and valves and the analytical procedure for the NO_x^- detection system are detailed in Table S1 (Section S4, ESI†). Briefly, reagents (sulfanilamide and N.E.D.) were introduced into the holding channel (H.C.) in specified proportions after the flow path of the chip was flushed by the sample/blank/standard, the sample/blank/standard and reagents in the H.C. were propelled to the reaction channel (R.C.) and then a specific reaction procedure was applied; subsequently there was the formation of a zone of product in the reaction channel which was propelled through the measurement cells and the absorbance was simultaneously calculated. The mixing method in this study is illustrated in detail in Section S5.1 and Fig. S5 of the ESI.†

3 Results and discussion

3.1 Optimization of SIA by orthogonal experiments

Three key parameters of the mixing method affect the mixing result: ratio, reciprocation and residence time, and the corresponding definitions are listed in Section S5.2 of the ESI.† Orthogonal experiments were conducted to analyze the effects of the three key parameters on the mixing and obtain the optimum parameters. The fluidic pathway was simplified and is shown in Fig. S6 (Section S5, ESI†) and the corresponding control procedures are listed in Table S2 (Section S4, ESI†).

Detailed system settings are provided in Section S5.3 of the ESI.† For convenient calculation and analysis, the maximum value of absorbance (MaxAbs) during the measurement was taken as the spectrophotometric result of each detection. The MaxAbs of different ratios, reciprocation and residence times are plotted in Fig. S7–S9 (Section S5, ESI†) and Fig. 1C. Fig. 1C shows that the MaxAbs rises (reddens) as the ratio increases, peaking at 8%, which is therefore set as the ratio of the SIA system. With this ratio, a downward tendency in the MaxAbs with increasing residence time for all reciprocations occurs in Fig. S8,† indicating the superfluousness of the residence time. In reference to reciprocation, as qualitatively and quantitatively shown in Fig. S9,† the MaxAbs remains steady with an increase in reciprocation, and all RSDs (relative standard deviations) are below 2%, demonstrating that the reciprocation is also not required in this method. From the analysis of the results of the orthogonal experiments, the ratio of 8% (80 μL for one detection) for each reagent was selected and steps for residence and reciprocation were omitted, which resulted in a decrease in the detection time and an improvement in the temporal resolution of the system. The total analysis time, including spectrum acquisition, injection and measurement (steps 3–7, Table S2, ESI†), is 3 min.

3.2 Effect of salinity on external LWCC

A 20 cm LWCC was connected to the chip as an external long absorption cell to carry out high-sensitivity detection and analyze the effect of salinity on this system. The corresponding fluidic pathway is shown in Fig. S10 (Section S6, ESI†) and the analytical steps are the same as those of the orthogonal experiment. 0, 0.5, 0.8, 1, 1.2, 1.5 μM nitrite standard solutions prepared with artificial seawater with the salinity range from 0–40 and an interval of 5 were used as the detection object. Absorbance over time of the above nitrite standard solutions with different salinities is shown in Fig. S11† and the corresponding linear curve fitting (CF) results over time are shown in Fig. S12.† The measurement frequency of absorbance is 2 Hz. *R* square (r^2) over time with different salinities is illustrated in Fig. S13.†

Fig. S12 and S13† show $r^2 > 0.99$ after 50 s, with the vast majority of them over 0.998, demonstrating the stability of the system during the measurement step. The time points at which the curves of the slope of different salinities in Fig. S12† reach the maximum are not synchronized, but all reach their maximum values after 100 s. To ensure the consistency of absorbance calculations for each detection during fluctuating salinities, two absorbance calculation methods (M1 and M2) were compared, and they are described mathematically as:

$$A_{M1} = A_t(t \geq 100) \quad (2)$$

$$A_{M2} = \frac{\sum_{i=100}^{t} A_i}{(t-99.5)/0.5} \quad (3)$$

where A is the absorbance, and t is the time point during the measurement step. In eqn (2), A_{M1} is the absorbance value at each time point and in eqn (3) A_{M2} represents the average of absorbance values from 100 s to each time point. Curves of the mean and RSD of the slopes calculated using M1 and M2 for each time point from 100 s to the end of the measurement for the nine salinities are shown in Fig. 2.

Results obtained from M2 are significantly more stable than those from M1. The RSD of the mean slopes from M2 (the solid black line in Fig. 2A) is 0.75% and the RSD of slopes from M2 (the solid red line in Fig. 2A) for the nine salinities hit a low of 3.57% at the end. Considering the measurement stability and consistency of data collection and in order to minimize the interference of salinity, the absorbance of each detection using the external 20 cm LWCC in the subsequent analysis was defined as the average of absorbance values from 100 s to the end of the measurement (133.5 s), *i.e.*,

$$A = \frac{\sum_{i=100}^{\text{EndTime}} A_i}{(\text{EndTime}-99.5)/0.5} \quad (4)$$

Fig. 2B provides the slopes and r^2 of the CF results from M2 at different salinities. The RSD of slopes with this method is less than 3.57% and all r^2 are greater than 0.997, suggesting that the interference of salinity is negligible, and the long optical path microfluidic system can be applied to natural waters with constant or fluctuating salinities.

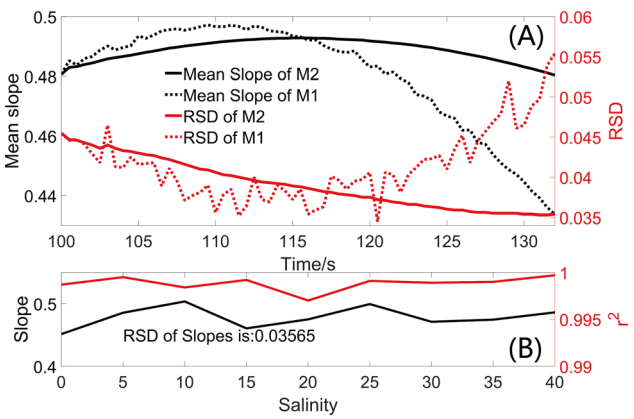

Fig. 2 (A) Variations of RSDs and mean slopes of M1 and M2 with detection time under flow detection. (B) Curve fitting results of standard curves at different salinities obtained with M2.

3.3 Performance

3 flushes were programmed after each detection to prevent measurements from the effect of carryover (Section S7, ESI†). At a salinity of 35, the LOD of nitrite is 0.015 μM for the 20 cm LWCC detection system and 0.0936 μM for the internal 5 cm detection system. The LOD calculation is presented in Section S8 of the ESI.† Based on the lengthening method of optical path in this study, the LOD was reduced by more than 6 times as the optical path length was increased by 4 times. Nitrite standard solutions with a concentration range of 0–3 μM and a salinity of 35 were measured with the 20 cm LWCC detection system and the results are illustrated in Fig. S17 and S18 (Section S8, ESI†). No linear relationship between nitrite concentration and absorbance exists for concentrations higher than 2 μM. For nitrite above 2 μM, the internal 5 cm cell can be used, which is linear up to 15 μM. The proposed method provides an approach with higher-sensitivity and lower LOD for microfluidic detection in the upper ocean of oligotrophic oceans where nitrite is generally present at nanomolar levels and the levels fluctuate over a narrow range.[27,46] This method offers a practical and effective high-sensitivity solution for the LoC-based detection of nutrients and other biochemical elements.

3.4 Long-term trial in the laboratory

A one-month automatic monitoring trial was implemented in the laboratory from June 30th to July 30th, 2023 to validate the long-term monitoring stability and accuracy of the 20 cm LWCC detection system as well as to determine

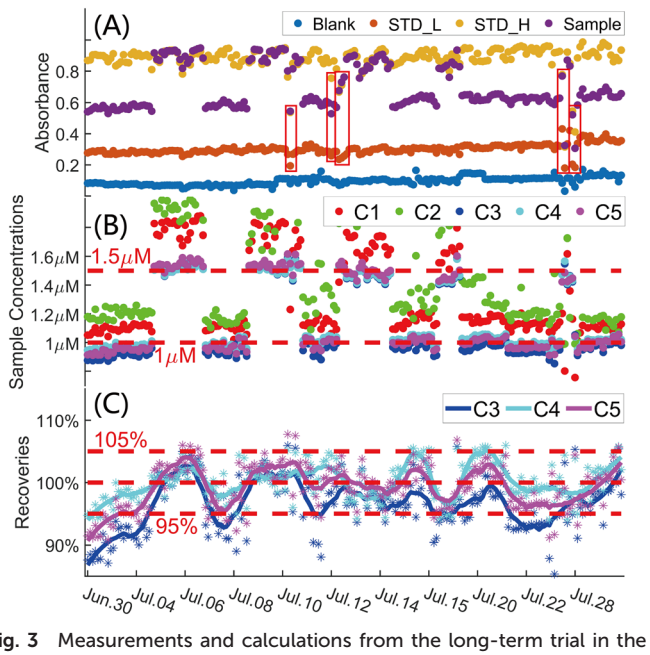

Fig. 3 Measurements and calculations from the long-term trial in the laboratory. (A) Absorbance of nitrite blank, standard solutions and samples. (B) Sample concentrations calculated with C1–C5. (C) Recoveries of C3, C4 and C5.

the calibration method and improve the data quality control of long-term autonomous detection. Experimental details and a photo of the long-term monitoring trial are shown in Section S9.1 of the ESI.† The automatic monitoring system performed 836 individual detections (209 blank detections, 209 STD_L detections, 209 STD_H detections and 209 sample detections) during the 30 days and all absorbances for all detections are shown in Fig. 3A. The absorbances of the detections during the measurement are shown in Fig. S20 (Section S9, ESI†).

Five calibration methods (C1–C5, Table S4, Section S9, ESI†) were applied to obtain the optimum and most accurate method for quality control during the long-term monitoring. Fig. 3B shows the sample detection results calculated using C1–C5 and demonstrates that the results calibrated using C3–C5 are closer to the real sample concentrations than C1 and C2. Recoveries of the long-term monitoring results obtained using C3–C5 are plotted in Fig. 3C. The differences among the recoveries of the three methods are minute. The recovery range of C4 is 94.01–105.96%, which shows the high accuracy during the long-term monitoring.[47,48] The mean concentration (Conc_m), mean recovery (Reco_m), weighted mean recovery (Reco_w), RSD and weighted RSD (RSD_w) of sample concentrations calculated using C3–C5 are listed in Table 1. The weighted mean recovery and weighted RSD of C4 are 100.11% and 3.10%, respectively, indicating an effective and stable calibration method for the one-month unattended monitoring by this system.

The absorbances in the red boxes in Fig. 3A plunge or spike, but the corresponding recoveries are between 95.38–104.40%. Absorbance and spectrum changes during the measurements of the nine detections are shown in Fig. S21 (Section S9, ESI†). Although the overall spectrum mutated and the absorbance throughout the measurements fluctuated during the nine detections, recoveries indicate that the results are not affected by the mutations and fluctuations. The long-term monitoring trial in the laboratory showed that the influence of spectral degradation (caused by minute bubbles, contamination on the detection channel wall or other factors) and salinity can be effectively eliminated by the absorbance calculation of M2 and steps 3 and 7 in Table S1,† and the stability and accuracy of the long-term monitoring can be realized by using the C4 calibration method.

3.5 Reduction of nitrate

Copperized cadmium granules (Shandong Puhuifen Chemical and Technology Co., Ltd., China) with size of 0.3–0.8 mm were placed in a silicone tube with an I.D. of 3 mm to make a 10 cm length cadmium reduction column. Detailed description of the reduction column and the reduction analysis are given in Section S3 of the ESI.† The system performs a reactivation after every 45 detections and the reactivation steps are listed in Table S3 (Section S4, ESI†).

3.6 Online analysis in the laboratory

Discrete surface water samples from 0–30 m were collected at six stations during a scientific cruise from September 18th to 23rd, 2023 in the Xisha Sea area of the South China Sea. Fig. S22 (Section S10, ESI†) provides the station locations. An SBE-911 CTD (Sea-Bird Electronics, Inc., USA) and a multi-parameter probe MINIpack CTD115M (Sea & Sun Technology, Germany) were used to acquire *in situ* temperature, salinity and chlorophyll a data during the sampling on this cruise. All water samples were filtered with 0.22 μm nylon membranes, and the NO_x^- concentrations of the filtered water samples were determined using the internal 5 cm cell and external 20 cm LWCC of the NO_x^- detection system in this study. Variations in temperature, salinity, NO_x^- concentrations and chlorophyll a (Chl a) with depth are shown in Fig. 4A.

The RSDs of each parameter at each station are shown in Fig. 4B. The RSD of salinity is below 1.1% and of temperature is below 4% at all stations, suggesting a slight vertical variation in salinity and temperature from 0–30 m at each station. A significant rise in RSDs was observed for NO_x^- and Chl a at S7 compared to other stations. In addition, Fig. 4A reveals that NO_x^- and Chl a vary considerably with depth at S7. S7 is located in a lagoon with an internal environment that is largely unaffected by external influences, has weak vertical mixing of the water column, and has uneven and variable vertical distributions of chlorophyll and nutrients. The correlations between each parameter and NO_x^- at each station are provided in Fig. 4C. The correlation coefficients at S7 are markedly higher than those at other stations, and that of Chl a reaches 0.93 and those of temperature and salinity are 0.89 and 0.58 respectively, indicating strong correlations among those parameters. Fig. 4D presents the r^2 between the RSDs of salinity, temperature and Chl a at all stations and their correlations with NO_x^-, *i.e.*, the relationship between

Table 1 Statistical data for C3, C4 and C5 from the long-term monitoring trial in the laboratory

Method number	Sample (μM)	Conc_m (μM)	Reco_m (%)	Reco_w (%)	RSD (%)	RSD_w (%)
C3	1	0.9497	94.97	96.61	4.27	3.90
	1.5	1.4921	99.47		3.24	
C4	1	1.0044	100.44	100.11	3.19	3.10
	1.5	1.4932	99.55		2.94	
C5	1	0.9816	98.16	99.15	3.66	3.48
	1.5	1.5132	100.88		3.16	

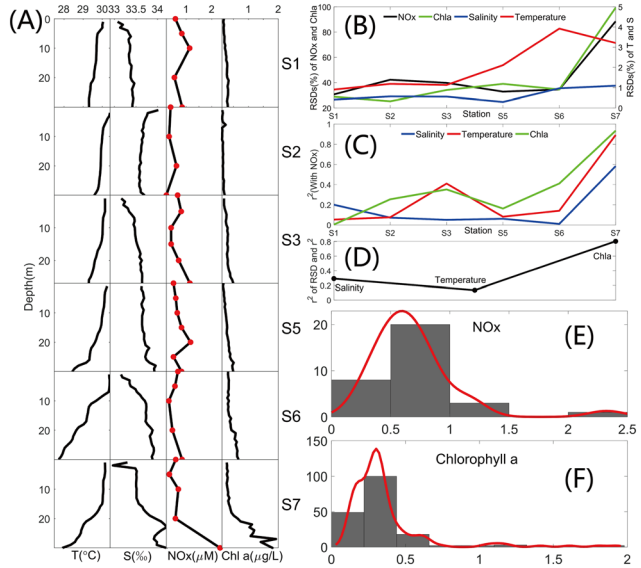

Fig. 4 (A) Variations in temperature (*T*), salinity (*S*), NO_x^- and Chl a with depth at each station of the scientific cruise in the Xisha Sea area. The red dots indicate the sampling depth. (B) RSDs for NO_x^-, Chl a, salinity and temperature at each station. (C) Correlations of NO_x^- with salinity, temperature and Chl a at each station. (D) r^2 between correlations of salinity, temperature and Chl a with NO_x^- and the corresponding RSD for all stations. (E and F) Statistical distribution of NO_x^- and Chl a for all stations of the scientific cruise in the Xisha Sea area.

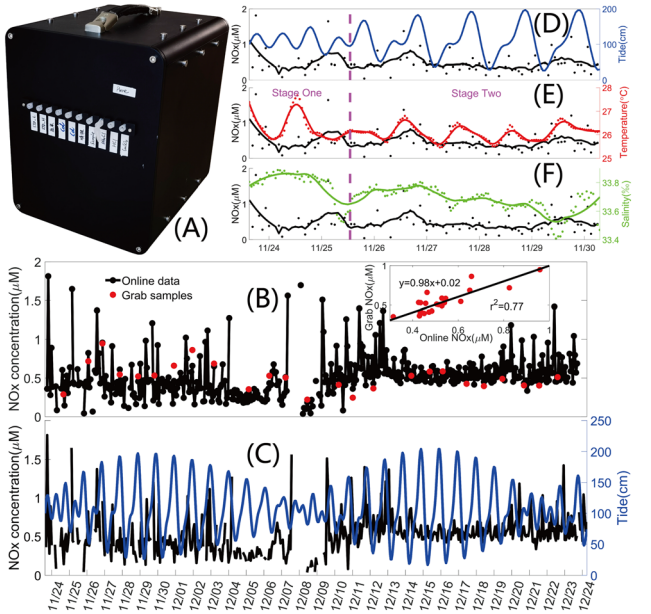

Fig. 5 (A) Photo of the portable analyzer prototype for online determination of NO_x^- in seawater. (B) All NO_x^- monitoring data over the one-month deployment at Sanya Station and NO_x^- concentrations of grab samples. The inset shows the curve fitting results between the online monitoring data and grab samples. (C) NO_x^- monitoring data and corresponding tide data. (D–F) Data comparisons between NO_x^- and tide, temperature and salinity at Sanya Station from November 23rd to November 30th, 2023.

the degree of variation for each parameter and its correlation with NO_x^-. r^2 between the Chl a variation and its correlation with NO_x^- reaches 0.8. The statistical distributions of Chl a and NO_x^- are plotted in Fig. 4E and F, and both have consistent patterns of distribution, which are concentrated in low levels.

Results of correlation and statistical analysis of data between the NO_x^- of water samples from the Xisha Sea area measured by the system developed in this study and other *in situ* data collected synchronously demonstrate that there is covariation between the growth of phytoplankton and nutrients in the surface water of this area, and they are strongly correlated.

3.7 Long-term unattended monitoring

A portable online analyzer prototype was developed and tested before the on-site deployment. The 3D design and a photo of the analyzer are shown in Fig. S23 (Section S11, ESI†) and Fig. 5A, respectively. The connection parts of the analyzer were all 3D-printed. All solutions were placed outside the analyzer and connected to the internal chip, pumps and valves *via* fittings and tubes.

The analyzer was deployed at the "Tropical Marine Biological Research Station in Hainan, South China Sea Institute of Oceanology, Chinese Academy of Sciences (Sanya, Hainan Province, China, abbreviated to Sanya Station)" from November 23rd to December 24th, 2023 to monitor the NO_x^- of the coastal water. The location of Sanya Station is shown in Fig. S24 (Section S11, ESI†). Culture tanks for various marine creatures are equipped at Sanya Station, which are filled with circulating and filtered (500 μm) seawater constantly pumped up from the coral reef area along the station. The analyzer was placed next to a mariculture tank for corals. A 5 μm 316 L stainless steel sintered filter was used to filter the seawater. As shown in Fig. S25 (Section S11, ESI†), a self-designed self-contained CTD was deployed in the tank to record the *in situ* salinity and temperature every minute. Discrete samples were manually collected during the deployment and measured with an AutoAnalyzer 3 continuous segmented flow analyzer (SEAL Analytical GmbH, Germany) at Sanya Station after the deployment for the validation of the analyzer's performance.

All NO_x^- monitoring data and grab samples data are illustrated in Fig. 5B, and data with concentrations below the limit of quantitation or above the upper limit of detection were excluded. The CF inset in Fig. 5B shows a significant correlation (slope = 0.98, r^2 = 0.77, N = 25) between the long-term online monitoring data and the grab samples. Fig. 5C shows the original NO_x^- one-month monitoring data and corresponding tide data from the National Marine Data Center of China (**https://mds.nmdis.org.cn/pages/tidalCurrent.html**). The NO_x^- is relatively stable and at a low level when the tide varies widely, and is at a high level and fluctuates sharply when the tide variation is small.

Salinity and temperature data are only available for the first week of the deployment (November 23rd to November 30th, 2023) due to the failure of the CTD (details shown in Section S11.1, ESI†). Data comparisons between NO_x^- and tide, temperature and salinity are shown in Fig. 5D–F, and the smooth curves derived by applying a Savitzky–Golay filter to the original data are used to show the trend for the data with narrow ranges and slight variations. NO_x^- is between 0.0426–1.8140 μM during the first week. The range of seawater salinity is 33.41–33.89‰ and its RSD is 0.31%, which is consistent with the results of the previous deployment at the Sanya Station.[44] The salinity of seawater in this area is stable, varying within a narrow range of less than 0.5‰. The seawater temperature range is from 25.46 to 27.67 °C and its RSD is 1.56%, the data rarely fluctuated and also ranged within a narrow range. The first week is divided into two stages by the magenta dashed line based on the tide fluctuation. The SD (standard deviation) for tide increases from 19.3168 to 48.7825 from Stage One to Stage Two, and the SDs for the original data of NO_x^-, temperature and salinity decrease from 0.4196, 0.5583 and 0.1007 to 0.2564, 0.3043 and 0.0861, respectively. Salinity, temperature and NO_x^- change opposite to tide level, which is in agreement with studies in estuaries and coastal waters.[15,18] No continental input is available in the sea area of Sanya Station and the temperature and salinity show stable physical properties for the seawater, and hence, dynamic processes of the biochemical elements in this area largely depend on the tide fluctuation. In Fig. 5F, the negative correlation between NO_x^- and salinity can be observed from the smooth curves for a salinity variation of less than 0.5‰ and a NO_x^- variation of less than 1.8 μM. This phenomenon is the same as that in studies with large variations in salinity and NO_x^-,[15,18,49] and the high-sensitivity of the method in this study was validated by the deployment in the sea area with low nutrient levels.

4 Conclusions

This work demonstrates the first application of a LWCC in LoC-based seawater nutrient devices. The modular off-chip LWCC with a screw joint in this study increases the optical path of the LoC system without changing the internal flow path of the microfluidic system and enables higher sensitivity, lower LOD and a wider detection range under the same micromixing conditions, and is low cost and easy to maintain and replace. The system is limited by low-throughput and high consumption of reagents. In the next stage, the high sensitivity method in this study will be integrated with high performance micromixers, miniature optical devices (LEDs and photodiodes), an on-chip actuation system, an incomplete chromogenic reaction and a high-throughput fluidic path to achieve a higher resolution *in situ* determination and provide data with more scientific value for marine science.

Data availability

Data for this article and ESI† are available at South China Sea Ocean Data Center at **https://data.scsio.ac.cn/**. Data title: High-sensitivity online microfluidic analyzer for nitrite and nitrate based on LWCC and SIA_experiments and applications.

Conflicts of interest

There are no conflicts to declare.

Acknowledgements

This work has received funding from the 2021 Open Fund for the Key Laboratory of Marine Environmental Survey Technology and Application, Ministry of Natural Resources of China (Grant: MESTA-2021-B006), the Guangdong Basic and Applied Basic Research Foundation (Grant: 2021A1515110639), the Hainan Provincial Natural Science Foundation of China (Grant: 422QN441), the Science and Technology Fundamental Resources Investigation Program (2022FY100601), the Science and Technology Planning Project of Guangzhou Nansha District Guangzhou City China (Grant: 2022ZD001), the Open Project Program (Grant: LTOZZ2003) of the State Key Laboratory of Tropical Oceanography (SCSIO, CAS) and the Research and Development Projects in Key Areas of Guangdong Province (Grant: 2020B1111020004). We sincerely thank Yuxian Liang, Qiutong Xu and Xingsheng Fu for their generous assistance during the deployment at the Tropical Marine Biological Research Station in Hainan, South China Sea Institute of Oceanology, Chinese Academy of Sciences.

References

1 G. Whitesides, *Lab Chip*, 2014, **14**, 3125–3126.
2 T. Fukuba and T. Fujii, *Lab Chip*, 2021, **21**, 55–74.
3 G. S. Clinton-Bailey, M. M. Grand, A. D. Beaton, A. M. Nightingale, D. R. Owsianka, G. J. Slavik, D. P. Connelly, C. L. Cardwell and M. C. Mowlem, *Environ. Sci. Technol.*, 2017, **51**, 9989–9995.
4 A. Jang, Z. Zou, K. K. Lee, C. H. Ahn and P. L. Bishop, *Meas. Sci. Technol.*, 2011, **22**, 032001.
5 G. Doku and S. Haswell, *Anal. Chim. Acta*, 1999, **382**, 1–13.
6 G. Greenway, S. Haswell and P. Petsul, *Anal. Chim. Acta*, 1999, **387**, 1–10.
7 R. Daykin and S. Haswell, *Anal. Chim. Acta*, 1995, **313**, 155–159.
8 H. Fiehn, S. Howitz, M. Pham, T. Vopel, M. Bürger and T. Wegener, *Micro Total Analysis Systems: Proceedings of the μTAS94 Workshop*, held at MESA Research Institute, University of Twente, The Netherlands, 21–22 November 1994, 1995, pp. 289–293.
9 J. Saez, R. Catalan-Carrio, R. M. Owens, L. Basabe-Desmonts and F. Benito-Lopez, *Anal. Chim. Acta*, 2021, **1186**, 338392.
10 R. Guijt and A. Manz, *Sens. Actuators, B*, 2018, **273**, 1334–1345.

11 Z. Li, H. Liu, D. Wang, M. Zhang, Y. Yang and T.-L. Ren, *TrAC, Trends Anal. Chem.*, 2022, 116790.
12 M. Mowlem, A. Beaton, R. Pascal, A. Schaap, S. Loucaides, S. Monk, A. Morris, C. L. Cardwell, S. E. Fowell and M. D. Patey, *et al.*, *Front. Mar. Sci.*, 2021, **8**, 697611.
13 A. D. Beaton, A. M. Schaap, R. Pascal, R. Hanz, U. Martincic, C. L. Cardwell, A. Morris, G. Clinton-Bailey, K. Saw and S. E. Hartman, *et al.*, *ACS Sens.*, 2022, **7**, 89–98.
14 A. J. Birchill, A. Beaton, T. Hull, J. Kaiser, M. Mowlem, R. Pascal, A. Schaap, Y. G. Voynova, C. Williams and M. Palmer, *Front. Mar. Sci.*, 2021, **8**, 698102.
15 A. M. Nightingale, S.-U. Hassan, B. M. Warren, K. Makris, G. W. Evans, E. Papadopoulou, S. Coleman and X. Niu, *Environ. Sci. Technol.*, 2019, **53**, 9677–9685.
16 A. M. Nightingale, A. D. Beaton and M. C. Mowlem, *Sens. Actuators, B*, 2015, **221**, 1398–1405.
17 J. Cleary, D. Maher and D. Diamond, in *Development and Deployment of a Microfluidic Platform for Water Quality Monitoring*, ed. S. C. Mukhopadhyay and A. Mason, Springer Berlin Heidelberg, Berlin, Heidelberg, 2013, pp. 125–148.
18 A. D. Beaton, C. L. Cardwell, R. S. Thomas, V. J. Sieben, F.-E. Legiret, E. M. Waugh, P. J. Statham, M. C. Mowlem and H. Morgan, *Environ. Sci. Technol.*, 2012, **46**, 9548–9556.
19 I. Ogilvie, V. Sieben, M. Mowlem and H. Morgan, *Anal. Chem.*, 2011, **83**, 4814–4821.
20 N. J. Petersen, K. B. Mogensen and J. P. Kutter, *Electrophoresis*, 2002, **23**, 3528–3536.
21 B. Lin, *Microfluidics: technologies and applications*, Springer, 2011, vol. 304.
22 H. Gai, Y. Li and E. S. Yeung, in *Optical Detection Systems on Microfluidic Chips*, ed. B. Lin, Springer Berlin Heidelberg, Berlin, Heidelberg, 2011, pp. 171–201.
23 T. Dallas and P. K. Dasgupta, *TrAC, Trends Anal. Chem.*, 2004, **23**, 385–392.
24 R. N. Páscoa, I. V. Tóth and A. O. Rangel, *Anal. Chim. Acta*, 2012, **739**, 1–13.
25 L. J. Gimbert and P. J. Worsfold, *TrAC, Trends Anal. Chem.*, 2007, **26**, 914–930.
26 L. A. Zimmer and G. A. Cutter, *Limnol. Oceanogr.: Methods*, 2012, **10**, 568–580.
27 L. Adornato, E. Kaltenbacher, T. Villareal and R. Byrne, *Deep Sea Res., Part I*, 2005, **52**, 543–551.
28 L. R. Adornato, E. A. Kaltenbacher, D. R. Greenhow and R. H. Byrne, *Environ. Sci. Technol.*, 2007, **41**, 4045–4052.
29 S. H. Cho, J. Godin and Y.-H. Lo, *IEEE Photonics Technol. Lett.*, 2009, **21**, 1057–1059.
30 C.-W. Wu and G.-C. Gong, *IEEE Sens. J.*, 2008, **8**, 465–469.
31 A. Datta, I.-Y. Eom, A. Dhar, P. Kuban, R. Manor, I. Ahmad, S. Gangopadhyay, T. Dallas, M. Holtz and H. Temkin, *et al.*, *IEEE Sens. J.*, 2003, **3**, 788–795.
32 R. Manor, A. Datta, I. Ahmad, M. Holtz, S. Gangopadhyay and T. Dallas, *IEEE Sens. J.*, 2003, **3**, 687–692.
33 D. Witters, N. Vergauwe, S. Vermeir, F. Ceyssens, S. Liekens, R. Puers and J. Lammertyn, *Lab Chip*, 2011, **11**, 2790–2794.
34 D. Decrop, E. P. Ruiz, P. T. Kumar, L. Tripodi, T. Kokalj and J. Lammertyn, *Microchip Diagnostics: Methods and Protocols*, 2017, pp. 85–101.
35 Z.-R. Xu, Y. Lan, X.-F. Fan and Q. Li, *Talanta*, 2009, **78**, 448–452.
36 X.-F. Fan, Q. Li, S.-L. Wang, Z.-R. Xu, W.-B. Du, Q. Fang and Z.-L. Fang, *Electrophoresis*, 2008, **29**, 4733–4738.
37 Y.-Z. Huang, W.-B. Du, J.-Z. Pan and Q. Fang, *Analyst*, 2008, **133**, 1237–1241.
38 S.-L. Wang, X.-F. Fan, Z.-R. Xu and Z.-L. Fang, *Electrophoresis*, 2005, **26**, 3602–3608.
39 W.-B. Du, Q. Fang, Q.-H. He and Z.-L. Fang, *Anal. Chem.*, 2005, **77**, 1330–1337.
40 S.-L. Wang, X.-J. Huang, Z.-L. Fang and P. K. Dasgupta, *Anal. Chem.*, 2001, **73**, 4545–4549.
41 M. J. Moorcroft, J. Davis and R. G. Compton, *Talanta*, 2001, **54**, 785–803.
42 J. Dutt and J. Davis, *J. Environ. Monit.*, 2002, **4**, 465–471.
43 P. Griess, *Ber. Dtsch. Chem. Ges.*, 1879, **12**, 426–428.
44 Z. Yang, C. Li, F. Chen, C. Liu, Z. Cai, W. Cao and Z. Li, *Mar. Chem.*, 2022, **245**, 104149.
45 P. Petsul, G. Greenway and S. Haswell, *Anal. Chim. Acta*, 2001, **428**, 155–161.
46 J. E. Dore and D. M. Karl, *Deep Sea Res., Part II*, 1996, **43**, 385–402.
47 Y. Gao, Z. Yu, L. Huang, Y. Zeng, X. Liu and D. Tang, *Anal. Chem.*, 2023, **95**, 9130–9137.
48 Y. Gao, J. Tang, Q. Zhou, Z. Yu, D. Wu and D. Tang, *Anal. Chem.*, 2024, **96**, 5014–5021.
49 O. Zielinski, D. Voß, B. Saworski, B. Fiedler and A. Körtzinger, *J. Sea Res.*, 2011, **65**, 456–460.